Available online at www.sciencedirect.com

ScienceDirect

International Journal of Solids and Structures 43 (2006) 7518–7533

INTERNATIONAL JOURNAL OF SOLIDS and STRUCTURES

www.elsevier.com/locate/ijsolstr

Quasi-static cylindrical cavity expansion in an elastoplastic compressible Mises solid

Rami Masri [*,1], David Durban

Faculty of Aerospace Engineering, Technion, Haifa 32000, Israel

Received 31 July 2005; received in revised form 6 March 2006
Available online 18 March 2006

Abstract

The self-similar elastoplastic field induced by quasi-static expansion of a pressurized cylindrical cavity is investigated for Mises solids under the assumption of plane-strain. Material behavior is modeled by the elastoplastic J_2 flow theory with the standard hypoelastic version. The theory accounts for elastic-compressibility and allows for arbitrary strain-hardening (or softening) in the plastic range. A formulation of the exact governing equations is presented and analyzed in detail for the remote elastic field and for asymptotic plastic behavior near the cavity wall, along with numerical investigations for the entire deformation zone. An analytical solution was obtained under the axially-hydrostatic assumption (axial stress coincides with hydrostatic stress) within an error of about 2% or less as compared to the exact, numerically evaluated, value of cavitation pressure. Two ad-hoc compressibility approximations for cavitation pressure are suggested. These relations, which give very accurate results, appear to provide tight lower and upper bounds on the exact value of cavitation pressure within an error of less than 0.5%.

Keywords: Cavity expansion; Cavitation; Compressible solid; Strain-hardening

1. Introduction

Axially-symmetric plane-strain deformation patterns around an internally pressurized cylindrical cavity, embedded in an elastoplastic solid, are of considerable interest in the mechanics of solids, as is the related spherical-symmetric behavior. For the extreme case of a small cavity embedded in an infinite medium, it is expected that the internal pressure will approach an asymptotic value known as the cavitation pressure (Hill, 1950; Durban and Baruch, 1976; Durban, 1979, 1988). That cavitation pressure defines the material resistance to cavity expansion and hence we refer to it also as the cavitation strength of the solid. The self-similar quasi-static spontaneous expansion induced by the cavitation pressure enables a simple analysis of the deformation pattern, according to the J_2 flow theory, with no need to trace the entire straining history

* Corresponding author. Tel.: +972 4 829 3805; fax: +972 4 829 2030.
E-mail address: masri@aerodyne.technion.ac.il (R. Masri).
[1] This work is based on a part of a Ph.D. thesis to be submitted to the Technion.

0020-7683/$ - see front matter
doi:10.1016/j.ijsolstr.2006.03.012

(Durban and Fleck, 1997; Durban and Papanastasiou, 1997; Durban and Masri, 2004; Masri and Durban, 2005, 2006). Hill (1950) derived approximate expressions for quasi-static spherical and cylindrical cavitation pressures based on compressible elastic/perfectly-plastic material response for both Tresca and Mises yield criteria. Closed form quadrature type solutions have been given by Durban and Baruch (1976), for quasi-static spherical cavitation in a compressible strain-hardening Mises material, and by Durban (1979) for quasi-static cylindrical cavitation in an incompressible Mises solid. These exact large strain solutions, are valid for any strain-hardening (or softening) characteristic. A more general cylindrical plane-strain analysis has been given by Durban and Kubi (1990) for plastic-orthotropic solids but with the neglect of elastic-compressibility. Elastic-compressibility has been considered in Durban (1988) where the J_2 deformation theory was employed. A general large strain quadrature type solution for the Tresca model was given in Durban and Kubi (1992) along with a corner solution. It is worth mentioning that quasi-static cavitation analysis is part of a more general dynamic analysis with a main application to penetration problems. Dynamic cavitation in metals was investigated by several authors for spherical and cylindrical cavity expansion patterns. A review of earlier work can be found in Masri and Durban (2005) for spherical cavitation and in Masri and Durban (2006) for cylindrical cavitation.

In this paper we examine the exact formulation (given in Section 2) of the equations governing quasi-static cylindrical cavitation in a compressible Mises medium under plane-strain constraint, for any strain-hardening characteristic. Material behavior is modeled by the elastoplastic J_2 flow theory with the standard hypoelastic form. The governing system consists of four coupled equations, for the three principal stresses and the radial velocity, and a separate equation for the density profile. An exact analytical solution for the governing equations system is not available in the literature. In fact, even existing numerical solutions (Durban, 1988; Forrestal et al., 1990; Luk and Amos, 1991) are for approximated models. We begin therefore, in Section 3, by analyzing in detail that system for the elastic deformation field, while in Section 4 we have explored the asymptotic behavior in the deep plastic zone near the cavity wall. In Section 5 we present a numerical solution of the governing system for several metals, and use the axially-hydrostatic assumption (axial stress coincides with hydrostatic stress) to derive an approximate analytical solution in terms of quadratures. Finally, in Section 6 two ad-hoc compressibility approximations for cylindrical cavitation pressure in compressible Mises media are suggested.

2. Self-similar quasi-static expansion of a cylindrical cavity

Consider a circular cylindrical cavity, of instantaneous radius A, expanding quasi-statically (with constant expansion velocity $\dot{A}$ sufficiently small to neglect inertia effects) under constant internal cavitation pressure p_c, in an infinite, remotely unstressed, elastoplastic compressible Mises medium. It is assumed that an axially-symmetric field is induced in the medium by the expanding cavity, and that a plane-strain deformation pattern is maintained by appropriate axial stresses.

Locating the origin (denoted by O in Fig. 1) of a cylindrical system (R, θ, Z), where R is the Eulerian radial coordinate, at the center of the cavity, there is just one equilibrium equation to be considered,

$$\frac{\mathrm{d}\sigma_r}{\mathrm{d}R} + \frac{1}{R}(\sigma_r - \sigma_\theta) = 0, \tag{1}$$

where $(\sigma_r, \sigma_\theta, \sigma_z)$ are the active Cauchy stresses. However, in steady-state expansion (cylindrical cavitation) we assume a self-similar deformation field with the nondimensional radial coordinate $\xi = R/A$ as the only independent variable (Fig. 1). Hence, it follows that (1) can be rewritten as

$$\Sigma_r' + \frac{1}{\xi}(\Sigma_r - \Sigma_\theta) = 0, \tag{2}$$

where $(\Sigma_r, \Sigma_\theta, \Sigma_z) = (\sigma_r, \sigma_\theta, \sigma_z)/E$ are the nondimensionalized stresses (with respect to the elastic modulus E) and differentiation with respect to ξ is denoted by a superposed prime. In fact, in the cavity expansion field the radial stress is monotonously increasing with ξ ($\Sigma_r' \geqslant 0$), so, from the equilibrium equation (2) it follows that $\Sigma_\theta > \Sigma_r$ in all of the deformation zone for quasi-static expansion.

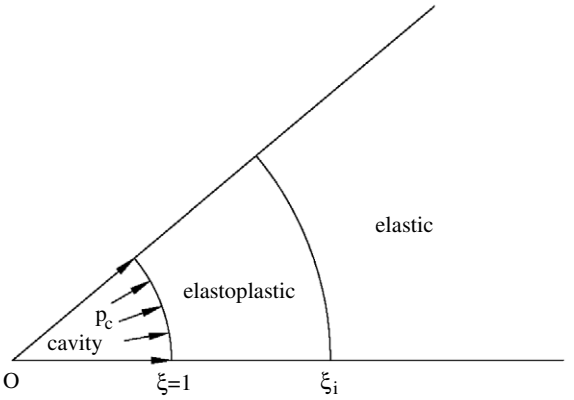

Fig. 1. Scheme of self-similar field in quasi-static expansion of a circular cylindrical cavity in compressible elastoplastic media. Cavitation pressure is p_c. The radial coordinate ξ is nondimensionalized with respect to the current radius of the cavity. Plastic yielding occurs at the elastic/plastic interface $\xi = \xi_i$. The remote boundary at infinity is stress-free.

The elastoplastic J_2 flow theory formulation can be written in the standard hypoelastic form

$$\mathbf{D} = \left(\frac{1+v}{E}\right)\overset{\circ}{\boldsymbol{\sigma}} - \left(\frac{v}{E}\right)(\mathbf{I}..\overset{\circ}{\boldsymbol{\sigma}})\mathbf{I} + \frac{3\dot{\epsilon}_p}{2\sigma_e}\mathbf{S}, \tag{3}$$

where a superposed dot denotes differentiation with respect to time. In (3) tensor $\mathbf{D}$ is the Eulerian strain rate, $\boldsymbol{\sigma}$ – the Cauchy stress tensor, $\overset{\circ}{\boldsymbol{\sigma}}$ – the Jaumann stress rate, $\mathbf{S}$ – the stress deviator, $\mathbf{I}$ – the second order unit tensor, v – Poisson's ratio and ϵ_p is the effective plastic strain and a known function of the Mises effective stress σ_e. The latter is defined by $\sigma_e = \sqrt{\frac{3}{2}\mathbf{S}..\mathbf{S}}$ which for an axially-symmetric field takes the nondimensionalized form

$$\Sigma = \frac{\sigma_e}{E} = \sqrt{\frac{1}{2}\left[(\Sigma_\theta - \Sigma_r)^2 + (\Sigma_\theta - \Sigma_z)^2 + (\Sigma_z - \Sigma_r)^2\right]}, \tag{4}$$

or, put differently,

$$\Sigma = \frac{\sqrt{3}}{2}\sqrt{(\Sigma_\theta - \Sigma_r)^2 + 3(\Sigma_z - \Sigma_h)^2}, \tag{5}$$

where Σ_h is the nondimensionalized hydrostatic stress

$$\Sigma_h = \frac{\sigma_h}{E} = \frac{1}{3}(\Sigma_r + \Sigma_\theta + \Sigma_z). \tag{6}$$

Also, the Eulerian strain rate components are simply

$$\dot{\epsilon}_r = \frac{d\dot{R}}{dR} = \left(\frac{\dot{A}}{A}\right)V', \quad \dot{\epsilon}_\theta = \frac{\dot{R}}{R} = \left(\frac{\dot{A}}{A}\right)\frac{V}{\xi}, \quad \dot{\epsilon}_z = 0, \tag{7}$$

where the axial strain rate $\dot{\epsilon}_z$ vanishes on account of the plane-strain constraint and $V = \dot{R}/\dot{A}$ is the nondimensional radial velocity, which describes the mathematical limit of quasi-static expansion.

Now, we introduce a useful transformation for the time derivative by the similarity relation (Durban and Fleck, 1997; Durban and Papanastasiou, 1997; Durban and Masri, 2004; Masri and Durban, 2005, 2006), namely

$$\dot{(\,)} = \dot{\xi}\frac{d(\,)}{d\xi} = \left(\frac{\dot{R}}{A} - \xi\frac{\dot{A}}{A}\right)\frac{d(\,)}{d\xi} = \frac{\dot{A}}{A}(V - \xi)\frac{d(\,)}{d\xi}. \tag{8}$$

Consequently, in the absence of material spin, the tensorial constitutive relation (3) separates into just three scalar equations, with the aid of (7) and (8),

$$V' = (V-\xi)\left\{[\Sigma_r - \nu(\Sigma_\theta + \Sigma_z)]' + \frac{3}{2}\frac{\Sigma_r - \Sigma_h}{\Sigma}\epsilon_p'\right\}, \tag{9}$$

$$\frac{V}{\xi} = (V-\xi)\left\{[\Sigma_\theta - \nu(\Sigma_z + \Sigma_r)]' + \frac{3}{2}\frac{\Sigma_\theta - \Sigma_h}{\Sigma}\epsilon_p'\right\}, \tag{10}$$

$$0 = (V-\xi)\left\{[\Sigma_z - \nu(\Sigma_r + \Sigma_\theta)]' + \frac{3}{2}\frac{\Sigma_z - \Sigma_h}{\Sigma}\epsilon_p'\right\}. \tag{11}$$

Relations (9)–(11), which appear to be highly nonlinear, are a particular case of a more comprehensive formulation for cylindrical deformation patterns in plastic pressure sensitive solids (Drucker–Prager constitutive model) considered by Durban and Papanastasiou (1997).

Finally, conservation of matter together with the plane-strain constraint require that

$$\frac{\dot\rho}{\rho} + \dot\epsilon_r + \dot\epsilon_\theta = 0, \tag{12}$$

where ρ is the density, so with the aid of (7) and (8), Eq. (12) transforms to

$$(V-\xi)\ln'\left(\frac{\rho}{\rho_0}\right) + V' + \frac{V}{\xi} = 0, \tag{13}$$

where ρ_0 is the reference density of the undeformed stress-free state.

To sum up, we have five governing equations in (2), (9)–(11) and (13) with five unknowns $(\Sigma_r, \Sigma_\theta, \Sigma_z, V, \rho)$ whose dependence on ξ should be determined using definitions (5) and (6). Integration of that system is carried from the cavity's wall ($\xi = 1$) where $V = 1$, to infinity ($\xi \to \infty$) where we have $\rho = \rho_0$ and both velocity and radial stress Σ_r should vanish. In fact, when no remote external loads are applied, we expect all stress components to vanish at infinity. Note however that this is not the case for dynamic cylindrical cavitation in an incompressible media as discussed by Masri and Durban (2006). Also, $P_c = -\Sigma_r$ ($\xi = 1$) denotes the nondimensionalized ($P_c = p_c/E$) cavitation pressure (or cavitation strength) (Fig. 1), determined by the solution.

In the present formulation, the effective plastic strain ϵ_p is a given function of Σ, which describes plastic strain-hardening (or softening), and we do not necessarily assume the existence of a definite yield point. For strain-hardening with a definite yield point, like the modified Ludwik power-hardening law, plastic response is activated at the elastic/plastic interface $\xi = \xi_i$ (Fig. 1), where ϵ_p vanishes and Σ reaches the value of the nondimensional yield stress Σ_y ($\Sigma_y = Y/E$ with Y denoting the yield stress). However, for strain-hardening response without a definite yield point, like the Ramberg–Osgood power-hardening law, the plastic branch is active within the entire deformation zone. In the special case of elastic/perfectly-plastic response ϵ_p is not known a priori and an extra algebraic equation is obtained from (4) or (5), in the post yield range,

$$\Sigma \equiv \Sigma_y. \tag{14}$$

Now, it is possible to express the density ρ in terms of the hydrostatic stress Σ_h by adding the three scalar constitutive relations (9)–(11), inserting the resulting sum in (13) and integrating over ξ to obtain

$$\rho = \rho_0 e^{-\Theta} \quad \text{with } \Theta = 3\beta\Sigma_h. \tag{15}$$

Here we use $\rho = \rho_0$ and $\Sigma_h = 0$ as stress-free conditions at infinity and take $\beta = 1 - 2\nu$ for the elastic-compressibility measure. Relation (15), which is identical with the density equation for spherical cavity expansion (Masri and Durban, 2005), can replace the matter conservation equation (13) to determine the density profile after solving for the stresses. In fact, (15) can be derived directly from (3) as a universal relation for any deformation pattern.

The constitutive equations are simplified if we subtract (10) from (9) and recast the result as

$$\ln'\left(1 - \frac{V}{\xi}\right) = -\left[(1+\nu)(\Sigma_\theta - \Sigma_r)' + \frac{3}{2}\frac{\Sigma_\theta - \Sigma_r}{\Sigma}\epsilon_p'\right] \tag{16}$$

with which we prefer to replace the constitutive relation (9). Thus, a simpler governing system, for quasi-static plane-strain cylindrical cavitation in an elastoplastic Mises solid, consists of four coupled equations ((2), (10), (11) and (16)) along with a separate relation for the density profile (15).

3. The elastic field

For solids with a definite yield point it is conceivable that at a distance from the cavity the strained medium will respond in a purely elastic deformation with $\epsilon_p \equiv 0$. For strain-hardening response without a definite yield point the plastic branch in the constitutive relations is active within the entire deformation zone but becomes negligible compared with the elastic branch when approaching infinity. With no active plastic branch the constitutive equations (10), (11) and (16) take the simpler form

$$\frac{V}{\xi} = (V-\xi)\big\{[\Sigma_\theta - \nu(\Sigma_z + \Sigma_r)]'\big\}, \tag{17}$$

$$0 = (V-\xi)\big\{[\Sigma_z - \nu(\Sigma_r + \Sigma_\theta)]'\big\}, \tag{18}$$

$$\ln'\left(1-\frac{V}{\xi}\right) = -(1+\nu)(\Sigma_\theta - \Sigma_r)'. \tag{19}$$

Integration of Eq. (18) gives the standard elastic relation

$$\Sigma_z = \nu(\Sigma_r + \Sigma_\theta), \tag{20}$$

since all three stresses should vanish at infinity. Likewise, the solution of the integrable equation (19) is

$$V = \xi\{1 - \exp[-(1+\nu)(\Sigma_\theta - \Sigma_r)]\}, \tag{21}$$

accounting for the condition that V should vanish at infinity where both stress components vanish alike. Now, inserting (20) and (21) back in (17) gives the constitutive relation in the circumferential direction

$$-\nu\Sigma_r' + (1-\nu)\Sigma_\theta' = \frac{1}{(1+\nu)\xi}\left[1 - e^{(1+\nu)(\Sigma_\theta - \Sigma_r)}\right]. \tag{22}$$

Eq. (22) along with the equilibrium equation (2) represent the elastic nonlinear coupled system for quasi-static cylindrical cavitation, under plane-strain conditions, with the stresses Σ_r and Σ_θ as unknowns. Using Eq. (20) we can find Σ_z while from (15) and (21) we can obtain the solutions for density ρ and velocity V, respectively.

The nonlinear equation (22) can be further simplified since for elastic response of common solids both $|\Sigma_r|$ and $|\Sigma_\theta|$ are extremely small by comparison with unity. Thus, we proceed with the linearized version

$$-\nu\Sigma_r' + (1-\nu)\Sigma_\theta' = -\frac{1}{\xi}(\Sigma_\theta - \Sigma_r), \tag{23}$$

which, together with (2), admit the simple solution

$$\Sigma_r = -\frac{C}{\xi^2} + B, \tag{24}$$

$$\Sigma_\theta = \frac{C}{\xi^2} + B, \tag{25}$$

where (B, C) are integration constants. The requirement that Σ_r vanishes at infinity gives $B = 0$ implying that Σ_θ vanishes as well at infinity, as we have assumed, and that both Σ_z from (20) and Σ_h from (6) vanish identically within the entire elastic zone.

To sum up, the quasi-static linear elastic solution is

$$\Sigma_r = -\frac{C}{\xi^2}, \quad \Sigma_\theta = \frac{C}{\xi^2}, \quad \Sigma_z \equiv \Sigma_h \equiv 0. \tag{26}$$

The radial material velocity follows from (21) and (26), under the assumption that $|\Sigma_r|, |\Sigma_\theta| \ll 1$, as

$$V = \xi(1+\nu)(\Sigma_\theta - \Sigma_r) = \frac{2(1+\nu)C}{\xi}, \tag{27}$$

while from (15) $\rho = \rho_0$ as the first order solution for the density. Since V should be positive we find from (27) that C must be positive as well. Therefore, it is clear from (26) that the intermediate axial stress assumption $\Sigma_r < \Sigma_z < \Sigma_\theta$ is valid in the elastic zone. For an incompressible material ($\nu = 1/2$), where $V = 1/\xi$, the value of

C must be $C = 1/3$. Knowing the value of C is useful also for numerical calculations of incompressible media because a shooting method is not needed. In general (for compressible materials) the integration constant C will be determined upon imposing continuity conditions at the elastic/plastic interface $\xi = \xi_i$. Finally, with the linear elastic steady-state solution (26) the effective stress (5) will take the simpler form

$$\Sigma = \frac{\sqrt{3}}{2}(\Sigma_\theta - \Sigma_r) = \frac{\sqrt{3}C}{\xi^2}. \tag{28}$$

4. Asymptotic analysis of the near cavity boundary layer

At the other extreme, the behavior of the thin layer adjacent to cavity wall ($\xi = 1$) is dominated by the plastic branch of the constitutive relations (9)–(11), so asymptotically as $\xi \to 1$ we obtain the near wall relations

$$V' = \frac{3}{2}(V - \xi)\frac{\Sigma_r - \Sigma_h}{\Sigma}\epsilon_p', \qquad \frac{V}{\xi} = \frac{3}{2}(V - \xi)\frac{\Sigma_\theta - \Sigma_h}{\Sigma}\epsilon_p', \tag{29}$$

$$0 = \frac{3}{2}(V - \xi)\frac{\Sigma_z - \Sigma_h}{\Sigma}\epsilon_p'. \tag{30}$$

From (30) the solution for the axial stress in the deep plastic field is

$$\Sigma_z = \Sigma_h \Rightarrow \Sigma_z = \Sigma_h = \tfrac{1}{2}(\Sigma_r + \Sigma_\theta). \tag{31}$$

Hence, we recover from (5) the simpler expression for the effective stress

$$\Sigma = \tfrac{\sqrt{3}}{2}(\Sigma_\theta - \Sigma_r), \tag{32}$$

where we have used the expected result $\Sigma_\theta > \Sigma_r$ along with (31).

By combining relations (29) and (31) we obtain the differential relation

$$\frac{dV}{V} = -\frac{d\xi}{\xi}, \tag{33}$$

which integrates, with $V(\xi = 1) = 1$, to the known incompressible velocity profile

$$V = \frac{1}{\xi}. \tag{34}$$

Introducing the plastic boundary layer radial coordinate $\delta = \xi - 1$, with $\delta \ll 1$, we find from (34) the boundary layer velocity profile

$$V \sim 1 - \delta. \tag{35}$$

Durban and Masri (2004) have shown that for spherical cavitation in Mises solids there is a similar expression $V \sim 1 - 2\delta$ which indicates that the spherical boundary layer is thinner than the cylindrical boundary layer. Inserting (31), (32) and (35) in the second of (29) and integrating over δ gives the asymptotic behavior of the effective plastic strain

$$\epsilon_p \sim \frac{1}{\sqrt{3}}\ln\left(\frac{1}{\delta}\right) \Longleftrightarrow \delta \sim e^{-\sqrt{3}\epsilon_p}, \tag{36}$$

indicating, as expected, extremely high levels of strain near the cavity. It is interesting to note that the leading term (36) is independent of material properties. The analogous expansion for the effective stress can be deduced from (36) since ϵ_p depends on Σ. For example, with the Ramberg–Osgood power law $\epsilon_p = K\Sigma^n$ we get

$$\Sigma \sim \left[\frac{1}{\sqrt{3}K}\ln\left(\frac{1}{\delta}\right)\right]^{1/n}, \tag{37}$$

where (K, n) are material parameters, and it can be seen that strain-hardening raises effective stress gradients within the boundary layer. Hence, it is expected that the boundary layer near the wall is extremely small for low strain-hardening metals and vanishes for elastic/perfectly-plastic behavior. In Section 5, the curves in Figs. 2–5 detailing Σ near the wall, corroborate expansion (37).

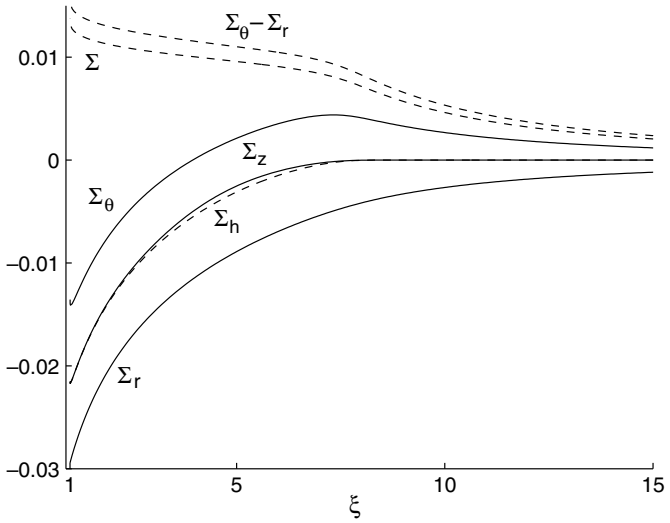

Fig. 2. Numerical quasi-static cylindrical cavitation solution for steel 5CrMoV. Metal characteristics are presented in Table 1. Strain-hardening behavior is modeled by the Ramberg–Osgood power-hardening law (41).

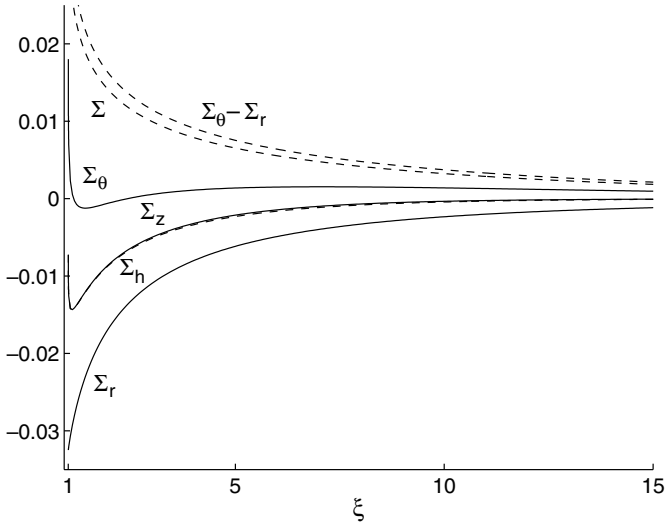

Fig. 3. Numerical quasi-static cylindrical cavitation solution for stainless steel. Metal characteristics are presented in Table 3. Strain-hardening behavior is modeled by the Ramberg–Osgood power-hardening law (41).

The effective plastic strain goes to infinity at the cavity's wall (36) so when strain-hardening is present the effective stress (37) is not bounded there and also Σ_θ (32) and $\Sigma_z = \Sigma_h$ (31) diverge at the wall. Hence the density (15) reduces to zero at the cavity's wall for compressible materials. However, for elastic/perfectly-plastic behavior, ρ reaches a finite value at the wall, because all stress components remain bounded there. The expression for the finite value density at the wall is therefore

$$\rho(\xi = 1) = \rho_0 \mathrm{e}^{(1-2\nu)(3P_c - \sqrt{3}\Sigma_y)}, \tag{38}$$

which is similar to the density value at a spherical cavity wall (Masri and Durban, 2005).

Using (2) together with (32) and (37) we write for the radial stress

$$\frac{\mathrm{d}\Sigma_r}{\mathrm{d}\delta} \sim \frac{2}{\sqrt{3}} \left[\frac{1}{\sqrt{3}K} \ln\left(\frac{1}{\delta}\right) \right]^{1/n}, \tag{39}$$

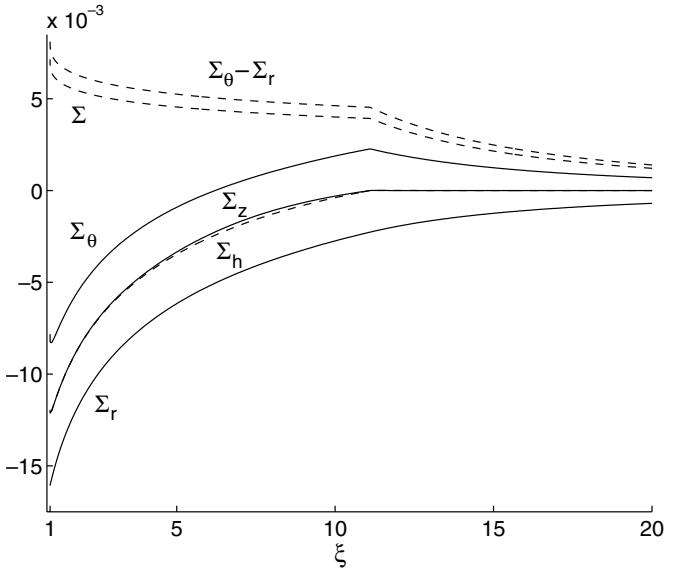

Fig. 4. Numerical quasi-static cylindrical cavitation solution for aluminum 5083-H131. Metal characteristics are presented in Table 2. Strain-hardening behavior is modeled by the modified Ludwik power-hardening law (42).

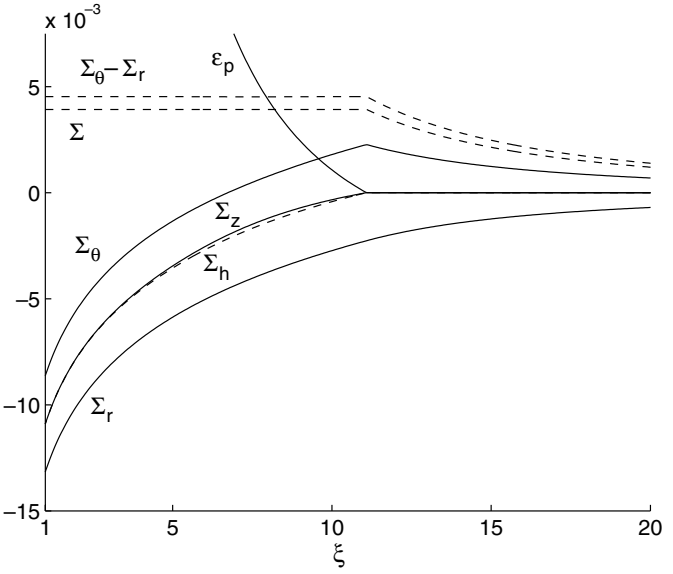

Fig. 5. Numerical quasi-static cylindrical cavitation solution for elastic/perfectly-plastic behavior of aluminum 5083-H131. Metal characteristics are presented in Table 2. Elastic/perfectly-plastic behavior is a special case of the modified Ludwik power-hardening law (42) with $n = \infty$.

and imposing the condition $\Sigma_r(\delta = 0) = -P_c$ leads to

$$\Sigma_r \sim -P_c + \frac{2}{\sqrt{3}} \int_0^{\delta} \left[\frac{1}{\sqrt{3}K} \ln\left(\frac{1}{\delta}\right) \right]^{1/n} d\delta \tag{40}$$

for the radial stress profile within the boundary layer.

5. Numerical solution and the axially-hydrostatic approximation

An exact analytical solution for the equations governing quasi-static plane-strain cylindrical cavitation, in a compressible Mises solid, is not available in the literature. In fact, even existing numerical solutions (Durban, 1988; Forrestal et al., 1990; Luk and Amos, 1991) are for approximated models. We begin therefore by presenting, in Figs. 2–5, numerical solutions of the complete system derived in Section 2. These numerical illustrations, obtained with a standard shooting method, will serve later as a data base of reference for further analytical derivations. We have chosen two hardening laws which, in the present notation, give the total elastoplastic strain $\epsilon = \Sigma + \epsilon_p$ as a function of the effective stress Σ. Thus, for the Ramberg–Osgood power-hardening law (Figs. 2 and 3)

$$\epsilon = \Sigma + K\Sigma^n, \quad \Sigma \geqslant 0, \tag{41}$$

while for the modified Ludwik power-hardening law (Figs. 4 and 5)

$$\begin{aligned} &\epsilon = \Sigma, \quad 0 \leqslant \Sigma \leqslant \Sigma_y, \\ &\epsilon = \Sigma_y\left(\frac{\Sigma}{\Sigma_y}\right)^n, \quad \Sigma \geqslant \Sigma_y. \end{aligned} \tag{42}$$

Note that both hardening laws reduce to elastic/perfectly-plastic behavior with $n = \infty$. Figs. 2 and 3 display numerical results for steel 5CrMoV and for stainless steel, respectively, while Figs. 4 and 5 show the numerical results for aluminum 5083-H131 and its elastic/perfectly-plastic version ($n = \infty$). The metal characteristics are summarized in Tables 1–3. The solid line curves illustrate the three active stress profiles while the effective and the hydrostatic stresses, along with the difference between circumferential and radial stresses, are presented by dashed lines. In Fig. 5 the effective plastic strain is also traced by a solid line as part of the elastic/perfectly-plastic solution.

While the expected tendency of Σ, Σ_θ, Σ_z and Σ_h towards infinity upon approaching the cavity's wall is clearly seen in Fig. 3, it is less apparent in Figs. 2 and 4, because the boundary layer near the wall is extremely thin for low strain-hardening metals. The expected tendency of ϵ_p towards infinity upon approaching the cavity's wall is observed in Fig. 5 for the elastic/perfectly-plastic version ($n = \infty$) of the aluminum alloy. It can be seen that differences between Σ_z and Σ_h are hardly noticeable, especially in the linear elastic zone and in the deep plastic zone. Calculated differences between the Mises effective stress Σ, defined in (5), and the expression $\frac{\sqrt{3}}{2}(\Sigma_\theta - \Sigma_r)$ are too small to be observed in all the deformation zone. It can be seen that the difference $\Sigma_\theta - \Sigma_r$, which is the highest stress difference, is greater than Σ and hence always positive.

Table 1
Low strain-hardening metal characteristics (Ramberg–Osgood power law)

Metal Reference	ST 5CrMoV Durban (1979)	ST AISI 4340 Durban (1979)	Titanium B120VCA Masri and Durban (2005)
E [GPa]	194	201	106
K	5.23×10^{31}	7.61×10^{54}	2.4×10^{29}
n	16.67	27.6	16.5
ν	0.26	0.28	1/3
P_c^{sp} (60)	3.440×10^{-2}	3.084×10^{-2}	4.397×10^{-2}
P_c^{inc} (63)	3.069×10^{-2}	2.751×10^{-2}	3.856×10^{-2}
$P_c^{\approx}$ (59)	3.003×10^{-2}	2.694×10^{-2}	3.797×10^{-2}
$P_c^{\dagger}$ (68)	2.946×10^{-2}	2.644×10^{-2}	3.743×10^{-2}
P_c^{cy}	2.943×10^{-2}	2.642×10^{-2}	3.737×10^{-2}
$P_c^{\perp}$ (69)	2.939×10^{-2}	2.639×10^{-2}	3.735×10^{-2}

Table 2
Low strain-hardening aluminum alloys characteristics (modified Ludwik power law)

Aluminum alloy Reference	5083-H131 Forrestal et al. (1990)	6061-T651 Luk et al. (1991)	7075-T651 Forrestal et al. (1992)
Y [MPa]	276	276	448
E [GPa]	70.3	68.9	73.1
Σ_y	0.392×10^{-2}	0.400×10^{-2}	0.613×10^{-2}
n	11.905	19.608	11.236
v	1/3	1/3	1/3
P_c^{sp} (60)	1.889×10^{-2}	1.764×10^{-2}	2.708×10^{-2}
P_c^{inc} (63)	1.653×10^{-2}	1.551×10^{-2}	2.370×10^{-2}
$P_c^{\approx}$ (59)	1.629×10^{-2}	1.527×10^{-2}	2.335×10^{-2}
$P_c^{\uparrow}$ (68)	1.608×10^{-2}	1.507×10^{-2}	2.303×10^{-2}
P_c^{cy}	1.607×10^{-2}	1.506×10^{-2}	2.302×10^{-2}
$P_c^{\downarrow}$ (69)	1.606×10^{-2}	1.505×10^{-2}	2.301×10^{-2}

Table 3
High strain-hardening metal characteristics (Ramberg–Osgood power law)

Metal Reference	AL killed steel Durban and Birman (1982)	Soft aluminum Durban and Birman (1982)	Stainless steel Masri and Durban (2005)
E [GPa]	207	69	206
K	6.43×10^{11}	1.27×10^{10}	5.78×10^{4}
n	4.505	3.718	3
v	0.27	0.33	0.30
P_c^{sp} (60)	0.552×10^{-2}	0.398×10^{-2}	3.938×10^{-2}
P_c^{inc} (63)	0.470×10^{-2}	0.334×10^{-2}	3.295×10^{-2}
$P_c^{\approx}$ (59)	0.466×10^{-2}	0.332×10^{-2}	3.274×10^{-2}
$P_c^{\uparrow}$ (68)	0.463×10^{-2}	0.331×10^{-2}	3.256×10^{-2}
P_c^{cy}	0.463×10^{-2}	0.331×10^{-2}	3.247×10^{-2}
$P_c^{\downarrow}$ (69)	0.463×10^{-2}	0.331×10^{-2}	3.246×10^{-2}

Now, following the numerical observations of Figs. 2–5, we suggest an approximate analytical solution in terms of quadratures, obtained by assuming that within the entire deformation zone

$$\Sigma_z = \Sigma_h \Rightarrow \Sigma_z = \Sigma_h = \frac{1}{2}(\Sigma_r + \Sigma_\theta), \tag{43}$$

which we label as the axially-hydrostatic approximation. This assumption is highly accurate in the linear elastic zone and in the deep plastic zone near the cavity's wall, as shown analytically in Sections 3 and 4 and clearly illustrated in Figs. 2–5. Notice also the slight difference between Σ_z and Σ_h in the transition zone between these two deformation fields. Approximation (43) contradicts of course the plane-strain constraint (11), unless $v = 1/2$, because it imposes only the vanishing of axial plastic strain. The error involved in that approximation will be discussed later in this section. For incompressible solids ($v = 1/2$) we obtain (43) from (11) as an exact relation, that imposes the vanishing of both axial elastic and plastic strains, which has been used by several authors. Exact solutions without any restrictions (except of incompressibility) have been suggested by Durban (1979) for quasi-static expansion and recently by Masri and Durban (2006) for dynamic cavitation.

As already discussed, a better approximation than (43) is $\Sigma = \frac{\sqrt{3}}{2}(\Sigma_\theta - \Sigma_r)$. In fact, this assumption simplifies the governing system, yet an analytical solution is still hard to find. However, by using assumption (43) the effective stress (5) takes the form

$$\Sigma = \frac{\sqrt{3}}{2}(\Sigma_\theta - \Sigma_r). \tag{44}$$

Substituting (44) and (43) in (2), (10) and (16) we arrive at the system of equations

$$\Sigma_{\mathrm{r}}' = \frac{2}{\sqrt{3}}\frac{\Sigma}{\xi}, \tag{45}$$

$$\frac{1}{\xi}\left(1+\frac{1}{\frac{V}{\xi}-1}\right) = \left[\left(1-\frac{1}{2}v\right)\Sigma_\theta - \frac{3v}{2}\Sigma_{\mathrm{r}}\right]' + \frac{\sqrt{3}}{2}\epsilon_{\mathrm{p}}', \tag{46}$$

$$\ln'\left(1-\frac{V}{\xi}\right) = -\left[\frac{2(1+v)}{\sqrt{3}}\Sigma + \sqrt{3}\epsilon_{\mathrm{p}}\right]'. \tag{47}$$

Integration of (47), on account of the stress-free conditions at infinity, gives for the velocity V

$$\frac{V}{\xi} = 1 - \frac{1}{\exp\left[\frac{2(1+v)}{\sqrt{3}}\Sigma + \sqrt{3}\epsilon_{\mathrm{p}}\right]}, \tag{48}$$

which satisfies the wall boundary condition $V(\xi=1)=1$ because, as shown by (36), $\epsilon_{\mathrm{p}}(\xi=1)\to\infty$. A further simplification of (46) is possible upon elimination of Σ_θ with the aid of the effective stress relation (44) and by inserting (48) with $v=\frac{1-\beta}{2}$ and $\epsilon=\Sigma+\epsilon_{\mathrm{p}}$, namely

$$\beta\Sigma_{\mathrm{r}}' + \frac{\beta}{2\sqrt{3}}\Sigma' + \frac{\sqrt{3}}{2}\epsilon' = \frac{1}{\xi}\left(1-\mathrm{e}^{\sqrt{3}\epsilon-\frac{\beta}{\sqrt{3}}\Sigma}\right). \tag{49}$$

This equation along with the equilibrium equation (45) construct a coupled nonlinear system with Σ and Σ_{r} as unknowns. By solving that system the solutions for V, Σ_θ, Σ_z and ρ can be obtained immediately from (48), (44), (43) and (15), respectively. Now, we derive a quadrature type solution for (45) and (49) starting with the differential relations

$$\frac{\sqrt{3}}{2}\frac{\mathrm{d}\Sigma_{\mathrm{r}}}{\Sigma} = \frac{\mathrm{d}\xi}{\xi}, \tag{50}$$

$$\beta\,\mathrm{d}\Sigma_{\mathrm{r}} + \frac{\beta}{2\sqrt{3}}\mathrm{d}\Sigma + \frac{\sqrt{3}}{2}\mathrm{d}\epsilon = \frac{\mathrm{d}\xi}{\xi}\left(1-\mathrm{e}^{\sqrt{3}\epsilon-\frac{\beta}{\sqrt{3}}\Sigma}\right). \tag{51}$$

Substituting (50) in (51) leads to

$$\mathrm{d}\Sigma_{\mathrm{r}} = -J\Sigma\,\mathrm{d}\Sigma, \tag{52}$$

where

$$J = J(\Sigma) = \frac{\frac{\mathrm{d}\epsilon}{\mathrm{d}\Sigma}+\frac{1}{3}\beta}{\mathrm{e}^{\sqrt{3}\epsilon-\frac{\beta}{\sqrt{3}}\Sigma}-1+\frac{2}{\sqrt{3}}\beta\Sigma} \tag{53}$$

is a function of Σ. Relation (52) is combined with (50) to give

$$\frac{2}{\sqrt{3}}\frac{\mathrm{d}\xi}{\xi} = -J\,\mathrm{d}\Sigma, \tag{54}$$

which together with (52) can be integrated in terms of quadratures. It appears that J is a basic function which reflects material and geometrical nonlinearities. Recalling from (37) that in the presence of strain-hardening $\Sigma(\xi=1)\to\infty$, and that $\Sigma_{\mathrm{r}}(\xi=1)=-P_{\mathrm{c}}$ (the quasi-static cavitation pressure) we arrive at the solution

$$\xi = \mathrm{e}^{Q}, \qquad \Sigma_{\mathrm{r}} = -P_{\mathrm{c}} + \int_{\Sigma}^{\infty} J(s)s\,\mathrm{d}s, \tag{55}$$

where

$$Q = \frac{\sqrt{3}}{2}\int_{\Sigma}^{\infty} J(s)\mathrm{d}s. \tag{56}$$

Notice that we do not necessarily assumed the existence of a definite yield point. This simplified the mathematical derivation and led to a unified treatment, gradually covering the entire elastoplastic behavior. Further simplification of the approximate solution can be achieved for elastic/perfectly-plastic behavior under the practical assumption $\Sigma_y \ll 1$. The differential relation (54) transforms ξ to Σ as the independent variable. Hence, an approximate solution for the location of the elastic/plastic interface ξ_i is

$$\ln(\xi_i^2) = \sqrt{3}\int_{\Sigma_y}^{\infty} J(\Sigma)\mathrm{d}\Sigma. \tag{57}$$

For the incompressible solid ($\beta = 0$) an exact expression of ξ_i can be obtained from (57) for any strain-hardening response with a definite yield point

$$\xi_i = \left(1 - \mathrm{e}^{-\sqrt{3}\Sigma_y}\right)^{-\frac{1}{2}}, \tag{58}$$

which, for $\Sigma_y \ll 1$, reduces to Hill's (1950) classical elastic/perfectly-plastic result $\xi_i = \left(\sqrt{3}\Sigma_y\right)^{-\frac{1}{2}}$. Hence, for an incompressible material the location of the elastic/plastic interface is independent of the hardening characteristics.

At infinity Σ and Σ_r vanish, so from the second of (55) we find the cavitation pressure

$$P_c^{\approx} = \int_0^{\infty} J\Sigma\,\mathrm{d}\Sigma = \int_0^{\infty} \frac{\left(\frac{\mathrm{d}\epsilon}{\mathrm{d}\Sigma} + \frac{1}{3}\beta\right)\Sigma\,\mathrm{d}\Sigma}{\mathrm{e}^{\sqrt{3}\epsilon - \frac{\beta}{\sqrt{3}}\Sigma} - 1 + \frac{2}{\sqrt{3}}\beta\Sigma}. \tag{59}$$

The latter is an approximation (hence denoted by the superscript $\approx$) for the quasi-static cylindrical cavitation pressure in a compressible Mises solid. A similar (exact) expression for the quasi-static spherical cavitation pressure has been obtained by Durban and Baruch (1976), as the asymptotic limit of the cavity expansion process under monotonously increasing internal pressure. That result has also been derived recently by Masri and Durban (2005) as the zeroth order solution in dynamic spherical cavitation analysis. The spherical cavitation pressure is brought here for the sake of comparison

$$P_c^{\mathrm{sp}} = \int_0^{\infty} \frac{\left(\frac{\mathrm{d}\epsilon}{\mathrm{d}\Sigma} + \beta\right)\Sigma\,\mathrm{d}\Sigma}{\mathrm{e}^{\frac{3}{2}\epsilon - \frac{\beta}{2}\Sigma} - 1 + 2\beta\Sigma}. \tag{60}$$

Approximations (57) and (59) can be used to derive specific expressions for elastic/perfectly-plastic materials by considering separately elastic ($\epsilon \equiv \Sigma$) and elastic/perfectly-plastic ($\Sigma \equiv \Sigma_y$) deformation zones. This procedure gives

$$\begin{aligned} \ln(\xi_i^2) &= \frac{1}{\left(1 - \frac{2}{\sqrt{3}}\beta\Sigma_y\right)} \ln\left[1 - \left(1 - \frac{2}{\sqrt{3}}\beta\Sigma_y\right)\mathrm{e}^{\frac{\beta-3}{\sqrt{3}}\Sigma_y}\right]^{-1}, \\ P_c &= \frac{\Sigma_y}{\sqrt{3}}\ln(\xi_i^2) + \int_0^{\Sigma_y} \frac{\left(1 + \frac{1}{3}\beta\right)\Sigma\,\mathrm{d}\Sigma}{\exp\left(\frac{3-\beta}{\sqrt{3}}\Sigma\right) - 1 + \frac{2}{\sqrt{3}}\beta\Sigma}, \end{aligned} \tag{61}$$

which take simpler, yet approximate, forms under the practical assumption $\Sigma_y \ll 1$

$$P_c = \frac{\Sigma_y}{\sqrt{3}}\left[1 + \ln(\xi_i^2)\right] \quad \text{with } \xi_i^2 = \left[\frac{\sqrt{3}}{(3+\beta)\Sigma_y}\right]. \tag{62}$$

While for an incompressible Mises solid ($\nu = \frac{1}{2} \Rightarrow \beta = 0$) approximation (59) reduces to the exact solution obtained by Durban (1979)

$$P_c^{\mathrm{inc}} = \int_0^{\infty} \frac{\Sigma\,\mathrm{d}\epsilon}{\mathrm{e}^{\sqrt{3}\epsilon} - 1}, \tag{63}$$

it does not reduce to the classical approximation for compressible elastic/perfectly-plastic solids obtained by Hill (1950)

$$P_c = \frac{\Sigma_y}{\sqrt{3}}\left[1 + \ln(\xi_i^2)\right] \quad \text{with } \xi_i^2 = \left[\frac{\sqrt{3}}{(3+2\beta)\Sigma_y}\right]. \tag{64}$$

The slight difference between the two solutions is in the location of the elastic/plastic interface, which affects the cavitation pressure, where instead of 2β in Hill's solution (64) there is just β in our solution (62).

In Tables 1–3 we compare the cavitation pressure P_c^{cy}, obtained from 'exact' numerical solutions, with the approximate expression (59) for several metals. The metals listed in Tables 1 and 3 are modeled by the Ramberg–Osgood power-hardening law for low (Table 1) and high (Table 3) strain-hardening response, while in Table 2 low strain-hardening aluminum alloys are modeled by the modified Ludwik power law. The accuracy of the numerical solution was tested by comparing with the exact solution for incompressible solids (63) which is also shown in the tables. Another useful check for the accuracy of the numerical procedure is through comparison with the exact value $P_c = \frac{\pi^2}{18}$ obtained from (63) for fully elastic behavior $\epsilon \equiv \Sigma$. By equating the effective stress for the elastic field (28) with Σ_y at the elastic/plastic interface ($\xi = \xi_i$) an approximate expression for C can be obtained using (57). That expression is useful in facilitating the numerical shooting method as a first intelligent guess for C.

The common conclusion that emerge from Tables 1–3, for nine different metals, is that $P_c^{\approx}$ is slightly above (up to 2%) the exact solution P_c^{cy}, while P_c^{inc} is above $P_c^{\approx}$ with a deviation of up to 4.5% from the exact solution. The latter result is expected since the assumption of incompressibility increases the strength of the solid. Also shown in the tables is the corresponding spherical cavitation pressure P_c^{sp} given by (60) which is in the range of 1.17–1.21 above the cylindrical cavitation pressure.

The error generated in replacing the plane-strain constraint (11) by assumption (43) can be assessed upon substituting (43) in (11) to obtain the elastic strain rate deviation

$$\psi(\xi) = -\beta(\xi - V)\Sigma_z'. \tag{65}$$

Or, with further use of the axially-hydrostatic assumption solution,

$$\psi(\Sigma) = -\frac{2\beta}{\sqrt{3}} e^{-\sqrt{3}\epsilon + \frac{\beta}{\sqrt{3}}\Sigma}\left(\Sigma - \frac{1}{\sqrt{3}J}\right). \tag{66}$$

Figs. 6–8 display $-\psi(\Sigma)$, which is positive in most of the deformation zone, for 5CrMoV steel alloy, stainless steel and 5083-H131 aluminum alloy, respectively. It is seen that the behavior of $\psi(\Sigma)$ for high strain-hardening materials with no definite yield point, like the stainless steel, is distinctive since the elastic branch is

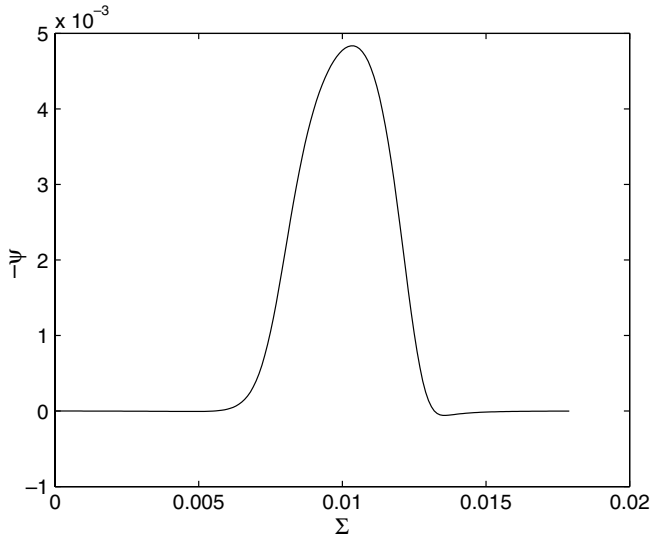

Fig. 6. Local deviation (error) from plane-strain constraint for 5CrMoV steel alloy.

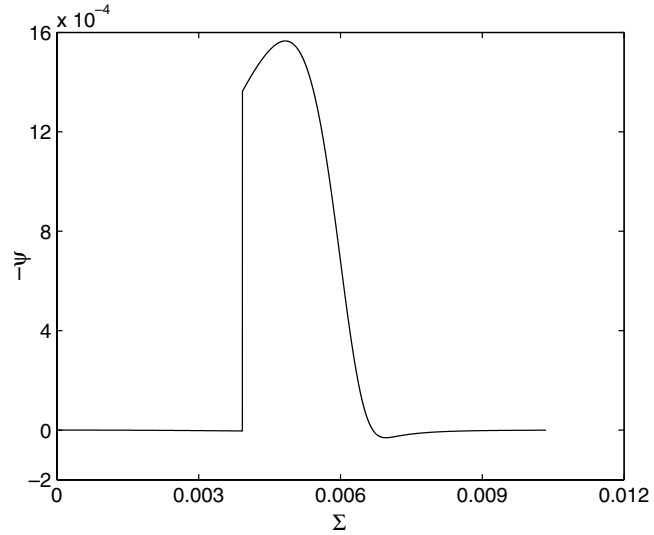

Fig. 7. Local deviation (error) from plane-strain constraint for 5083-H131 aluminum alloy.

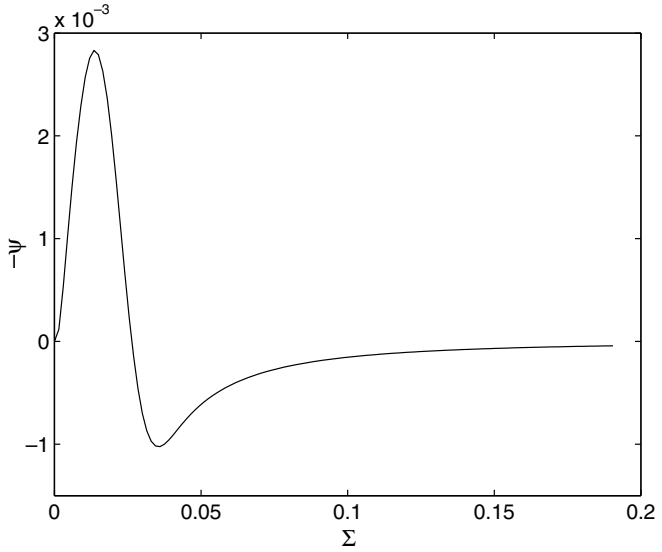

Fig. 8. Local deviation (error) from plane-strain constraint for stainless steel.

dominant only in a very small range of Σ. In all examples, however, the magnitude of the error ψ reflects the difference between Σ_z and Σ_h illustrated in Figs. 2–5.

We can summarize this section by the conclusion that the axially-hydrostatic approximation provides a better prediction, of the cylindrical cavitation pressure, than the widely used incompressible model.

6. Two ad-hoc compressibility approximations

Recalling that approximation (59) is above the accurate numerical result (P_c^{cy}), we suggest an artificial increase of elastic-compressibility to reduce the cavitation strength. To this end we replace ν, in (10) and (16), with $\frac{1-\beta^*}{2}$, where $\beta^* > \beta$. Following the same reasoning as for the axially-hydrostatic approximation we arrive at the cavitation pressure

$$P_c^* = \int_0^\infty \frac{\left(\frac{d\epsilon}{d\Sigma} + \frac{\beta^*}{3}\right)\Sigma\, d\Sigma}{e^{\sqrt{3}\epsilon - \frac{\beta^*}{\sqrt{3}}\Sigma} - 1 + \frac{2}{\sqrt{3}}\beta^*\Sigma}. \tag{67}$$

Now, for elastic/perfectly-plastic response, with $\Sigma_y \ll 1$, we recover from (67) Hill's classical approximation (64) when $\beta^* = 2\beta$. The corresponding cavitation pressure

$$P_c^{\uparrow} = \int_0^\infty \frac{\left(\frac{d\epsilon}{d\Sigma} + \frac{2}{3}\beta\right)\Sigma\, d\Sigma}{e^{\sqrt{3}\epsilon - \frac{2}{\sqrt{3}}\beta\Sigma} - 1 + \frac{4}{\sqrt{3}}\beta\Sigma} \tag{68}$$

appears (Tables 1–3) as a better approximation than $P_c^{\approx}$ though still higher (hence denoted by the superscript $\uparrow$) than P_c^{cy}, with a deviation that consistently is less than 0.5%.

On the basis of the approximate expressions (59) and (68) we examine a similar relation for cylindrical cavitation pressure, namely

$$P_c^{\downarrow} = \int_0^\infty \frac{\left(\frac{d\epsilon}{d\Sigma} + \frac{2}{3}\beta\right)\Sigma\, d\Sigma}{e^{\sqrt{3}\epsilon - \frac{\beta}{\sqrt{3}}\Sigma} - 1 + \sqrt{3}\beta\Sigma}, \tag{69}$$

which gives (Tables 1–3) uniformly lower values (hence denoted by the superscript $\downarrow$) than the exact values (P_c^{cy}), with a deviation of less than 0.5%. As for the upper bound (68), Hill's approximation (64) can be deduced also from (69) when $\Sigma_y \ll 1$. Actually, it can be shown that the three-parameter expression

$$P_c = \int_0^\infty \frac{\left(\frac{d\epsilon}{d\Sigma} + \frac{\kappa_2}{3}\beta\right)\Sigma\, d\Sigma}{e^{\sqrt{3}\epsilon - \frac{\kappa_1}{\sqrt{3}}\beta\Sigma} - 1 + \frac{\kappa_3}{\sqrt{3}}\beta\Sigma} \tag{70}$$

reduces to Hill's approximation (64), for $\Sigma_y \ll 1$, when

$$\kappa_2 = \kappa_3 - \kappa_1 = 2. \tag{71}$$

Yet, the possibility of choosing a best fit value for κ_3 in the range of 3 ($P_c^{\downarrow}$ (69)) to 4 ($P_c^{\uparrow}$ (68)) is not explored further. The upshot of this section are practical bounds on the cylindrical cavitation pressure in compressible Mises solids

$$P_c^{\downarrow} < P_c^{cy} < P_c^{\uparrow} (< P_c^{\approx}). \tag{72}$$

7. Concluding remarks

Most of existing literature on cavitation phenomena in elastoplastic solids is dominated by spherical deformation patterns. In this study we have presented a detailed numerical and analytical analysis of quasi-static plane-strain cylindrical cavitation fields in Mises type solids. The axially-hydrostatic assumption was investigated in detail and an analytical solution was obtained under this assumption within an error of about 2% or less above the exact cavitation pressure. On the basis of the axially-hydrostatic approximate solution two ad-hoc compressibility approximations were suggested ((68) and (69)). Comparison with exact numerical results points that these relations, which give very accurate results, appear to provide practical tight bounds on the exact value of cavitation pressure within an error of about 0.5% or less. Hopefully, establishing cylindrical cavitation analysis on equal footing with existing spherical cavitation studies, will provide a better understanding of indentation and penetration phenomena.

Acknowledgements

One of us (D.D) wishes to acknowledge the support of the Sydney Goldstein Chair in Aerospace Engineering. Part of this study was supported by the fund for the promotion of research at the Technion.

References

Durban, D., 1979. Large strain solution for pressurized elasto/plastic tubes. J. Appl. Mech. 46, 228–230.
Durban, D., 1988. Finite straining of pressurized compressible elasto-plastic tubes. Int. J. Engng. Sci. 26, 939–950.
Durban, D., Baruch, M., 1976. On the problem of a spherical cavity in an infinite elasto-plastic medium. J. Appl. Mech. 43, 633–638.
Durban, D., Birman, V., 1982. On the elasto-plastic stress concentration at a circular hole in an anisotropic sheet. Acta Mech. 43, 73–84.
Durban, D., Fleck, N.A., 1997. Spherical cavity expansion in a Drucker–Prager solid. J. Appl. Mech. 64, 743–750.
Durban, D., Kubi, M., 1990. Large strain analysis for plastic-orthotropic tubes. Int. J. Solids Struct. 26, 483–495.
Durban, D., Kubi, M., 1992. A general solution for the pressurized elastoplastic tube. J. Appl. Mech. 59, 20–26.
Durban, D., Masri, R., 2004. Dynamic spherical cavity expansion in a pressure sensitive elastoplastic medium. Int. J. Solids Struct. 41, 5697–5716.
Durban, D., Papanastasiou, P., 1997. Cylindrical cavity expansion and contraction in pressure sensitive geomaterials. Acta Mech. 122, 99–122.
Forrestal, M.J., Luk, V.K., Brar, N.S., 1990. Perforation of aluminum armor plates with conical-nose projectiles. Mech. Mater. 10, 97–105.
Forrestal, M.J., Luk, V.K., Rosenberg, Z., Brar, N.S., 1992. Penetration of 7075-T651 aluminum targets with ogival-nose rods. Int. J. Solids Struct. 29, 1729–1736.
Hill, R., 1950. The Mathematical Theory of Plasticity. Oxford University Press, London.
Luk, V.K., Amos, D.E., 1991. Dynamic cylindrical cavity expansion of compressible strain-hardening materials. J. Appl. Mech. 58, 334–340.
Luk, V.K., Forrestal, M.J., Amos, D.E., 1991. Dynamic spherical cavity expansion of strain-hardening materials. J. Appl. Mech. 58, 1–6.
Masri, R., Durban, D., 2005. Dynamic spherical cavity expansion in an elastoplastic compressible Mises solid. J. Appl. Mech. 72, 887–898.
Masri, R., Durban, D., 2006. Dynamic cylindrical cavity expansion in an incompressible elastoplastic medium. Acta Mech. 181, 105–123.